Available online at www.sciencedirect.com

ScienceDirect

Mendeleev Commun., 2021, **31**, 887–889

Mendeleev Communications

Luminescence and optical absorption of fluorozirconate glass doped with K_2MnF_6

Maria N. Brekhovskikh,*[a] Sergey Kh. Batygov,[b] Liudmila V. Moiseeva,[b] Maxim V. Mastryukov[a] and Konstantin S. Nikonov[a]

[a] *N. S. Kurnakov Institute of General and Inorganic Chemistry, Russian Academy of Sciences, 119991 Moscow, Russian Federation. E-mail: mbrekh@igic.ras.ru*

[b] *Prokhorov General Physics Institute, Russian Academy of Sciences, 119991 Moscow, Russian Federation*

DOI: 10.1016/j.mencom.2021.11.040

Fluorozirconate glass doped with K_2MnF_6 was produced to obtain a red-emitting phosphor, and K_2MnF_6 was synthesized according to a specially developed procedure using xenon difluoride. The luminescence spectrum exhibited a band at 550 nm attributed to Mn^{2+}, and the absorption spectra belonged to Mn^{2+} and Mn^{3+} ions, which were formed due to the reduction of Mn^{4+} ions.

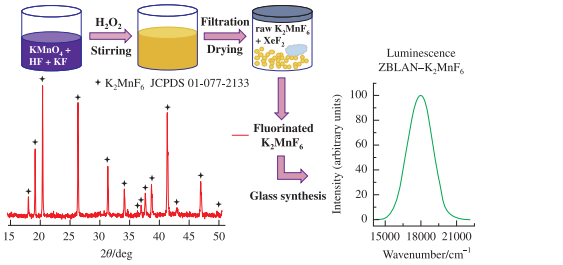

Keywords: fluorozirconate glass, manganese ions, fluorination with XeF_2, luminescence, optical absorption.

At present, phosphor-converted white light-emitting diodes (LEDs) do not have any alternative for use in household lighting because they surpass other sources of white light in many parameters. Ordinary white LEDs contain a blue LED as a primary radiation source and, typically, a yellow emitting phosphor, such as a garnet $Y_3Al_5O_{12}:Ce^{3+}$ (YAG:Ce).[1] To obtain warm white light with a high color rendering index, it is necessary to add an intense red phosphor, effectively excited by blue radiation emitted by the LED. Among well-known activators, manganese ions of different valences can emit red light in a properly chosen solid-state environment. A new generation of saturated red fluoride phosphors using Mn^{4+} as an activator has gained attention in enhancing the color rendering properties and efficiency of white LEDs.[2] Crystalline fluoride hosts were proposed for Mn^{4+}-doped phosphors due to the fact that Mn^{4+} emission in fluorides is close to an optimal wavelength near 630 nm for the red phosphor.[3–10] However, these fluoride phosphors are sensitive to high temperature and humidity.[11]

Fluorozirconate glasses of the ZrF_4–BaF_2–LaF_3–AlF_3–NaF (ZBLAN) system are attractive materials for technology due to the non-toxicity of components, relatively simple synthesis procedures, and unique optical properties.[12,13] In this work, we investigated the activation of fluorozirconate glass with Mn^{4+} ions to obtain red luminescence. A fluoride precursor K_2MnF_6 for red phosphors was used as a source of Mn^{4+}.

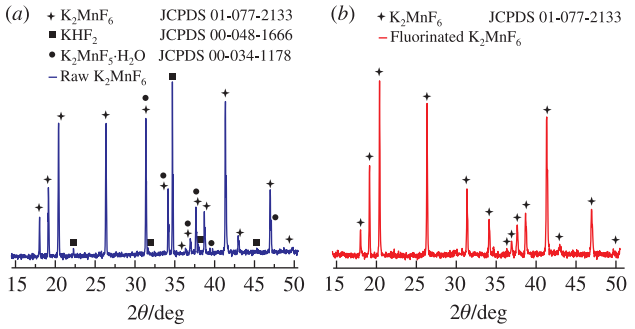

Figure 1 (*a*) XRD pattern of the synthesized K_2MnF_6 containing KHF_2 and $K_2MnF_5·H_2O$ impurities; (*b*) XRD pattern of the sample after heat treatment with XeF_2.

The glasses were synthesized from a starting fluoride mixture with the batch composition $55.8ZrF_4·14.4BaF_2·6LaF_3·3.8AlF_3·20NaF$ by melting the components in stoichiometric amounts at 850–900 °C in an atmosphere of argon.

The hexafluoromanganate dopant was synthesized in accordance with a published procedure[14] using the reaction:

$$2KMnO_4 + 2KF + 10HF + 3H_2O_2 \rightarrow 2K_2MnF_6 + 8H_2O + 3O_2. \quad (1)$$

The golden yellow precipitate of K_2MnF_6 was kept in a vacuum at 100 °C for 5 h until the formation of anhydrous K_2MnF_6. Figure 1 shows the X-ray diffraction (XRD) patterns† of the synthesized raw K_2MnF_6 powders and fluorinated K_2MnF_6 measured at 2θ ranging from 15 to 50°. As can be seen, the raw K_2MnF_6 after synthesis contained the main impurities of $K_2MnF_5·H_2O$ and KHF_2. At the second stage, we used xenon difluoride for the preparation of anhydrous K_2MnF_6 as described previously.[15] To remove oxygen-containing impurities and the concomitant compound KHF_2, the precursor K_2MnF_6 sample was heat treated in an atmosphere of xenon difluoride at 300 °C for 2 h according to the following reactions:

$$K_2MnF_5 + 0.5XeF_2 \rightarrow K_2MnF_6 + 0.5Xe, \quad (2)$$

$$K_2MnF_5·H_2O + 1.5XeF_2 \rightarrow K_2MnF_6 + 1.5Xe + 2HF + 0.5O_2. \quad (3)$$

The XRD data indicated that a single-phase sample of K_2MnF_6, which crystallizes in the hexagonal system [space group, $P6_3mc$; lattice parameters a = 5.719(1) and c = 9.33(3) Å, C = 1.6314, and Z = 2 (PDF JCPDS 01-077-2133)] was obtained as a result of

† The XRD patterns were determined at room temperature with a Bruker D8 Advance diffractometer (Ni-filtered CuKα radiation, LYNXEYE detector).

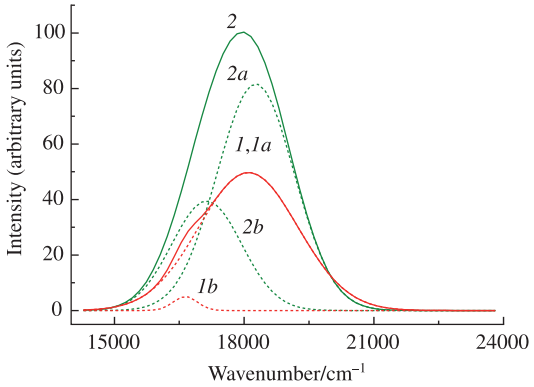

Figure 2 Luminescence spectra of (*1*) ZBLAN–K_2MnF_6 (0.1 mol%) and (*2*) ZBLAN–K_2MnF_6 (1 mol%) glasses. Spectra *1* and *2* were decomposed into two Gaussian sub-bands *1a*, *1b* and *2a*, *2b*, respectively.

the synthesis with additional heat treatment in an atmosphere of xenon difluoride.

For optical studies, the samples of glasses doped with K_2MnF_6 at a concentration of 0.1–1 mol% were fabricated as small rods with a diameter of 5 mm and polished.

The luminescence spectra[‡] demonstrated a single band at 550 nm due to the transition $^4T_1(G) \rightarrow {}^6A_1$ in Mn^{2+} ions (Figure 2). The emission band maximum is shifted from 18100 cm^{-1} at 0.1 mol% K_2MnF_6 to 17970 cm^{-1} at 1 mol% K_2MnF_6; this can be due to a change in the concentration ratio between different manganese centers. An increase in the total concentration of manganese led to an increase in the fraction of complex activator centers with transition energies lower than that of single centers to cause a band shift to lower energies.

Figure 2 shows the luminescence spectra decomposed into Gaussian sub-bands. At 0.1 mol% K_2MnF_6 [Figure 2 (spectrum *1*)], the intensity of low-energy component (band *1b)* was small; therefore, the luminescence band maximum almost coincided with the maximum of a high-energy component (band *1a*) caused by single Mn^{2+} ions due to the predominance of these ions at 0.1 mol% K_2MnF_6. At 1 mol% K_2MnF_6 [Figure 2 (spectrum *2*)], the intensity low-energy component (band *2b)* was comparable to that of the high-energy component (band *2a*); therefore, the luminescence band maximum was shifted to lower energies.

The absorption spectrum[§] of ZBLAN–K_2MnF_6 (1 mol%) glass (Figure 3) demonstrated bands at 330–350 and 400 nm caused by transitions from the $^6A_1$ ground level to $^4E(D)$, $^4T_2(D)$ and $^4A_1$,$^4E(G)$ levels in the Mn^{2+} ion and a broad band at 420–430 nm

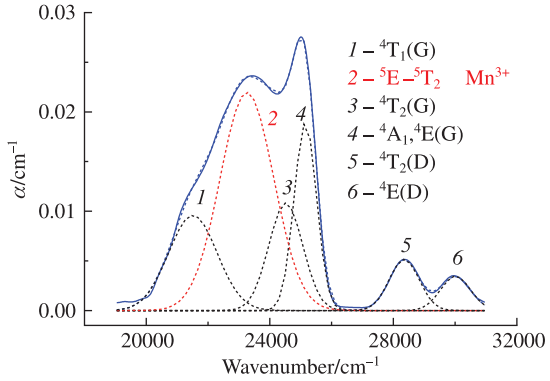

Figure 3 Absorption spectrum of ZBLAN–K_2MnF_6 (1 mol%) glass.

‡ The luminescence spectra were recorded with an SDL-1 spectrometer at room temperature. To excite luminescence, we used a LED emitting at 400 nm; full width at half maximum (FWHM), 16 nm.

§ Absorption spectra of the glasses were measured with a Cary 5000 spectrophotometer in a range of 300–600 nm at room temperature.

Table 1 Absorption bands in the spectrum of ZBLAN–K_2MnF_6 (1 mol%).

ν/cm^{-1}	λ/nm	Ion	Transition
30012 (30598)	333 (327)	Mn^{2+}	$^6A_1 \rightarrow {}^4E(D)$
28354 (29369)	353 (340)	Mn^{2+}	$^6A_1 \rightarrow {}^4T_2(D)$
25146	398	Mn^{2+}	$^6A_1 \rightarrow {}^4A_1$, $^4E(G)$
24469 (24180)	409 (414)	Mn^{2+}	$^6A_1 \rightarrow {}^4T_2(G)$
23221	431	Mn^{3+}	$^5E \rightarrow {}^5T_2$
21558	464	Mn^{2+}	$^6A_1 \rightarrow {}^4T_1(G)$

partially overlapped with a band at 400 nm. The broad band masks two absorption bands of Mn^{2+} corresponding to transitions to the $^4T_1(G)$ and $^4T_2(G)$ levels.

The absorption spectrum shown in Figure 3 was decomposed into six Gaussian components: five bands due to transitions in the Mn^{2+} ion and a broad band at 430 nm. In this absorption band, the luminescence from Mn^{2+} was very weak and most likely excited due to overlap with the neighbor absorption bands of Mn^{2+}. Luminescence from Mn^{4+} was not excited. This fact allowed us to ascribe the broad absorption band to Mn^{3+} ions, which are formed due to incomplete reduction of Mn^{4+} ions. The absorption spectrum of Mn^{3+} observed in the studied spectral range is consistent with published data.[16–18] The absorption bands and the corresponding electron transitions in the Mn^{2+} and Mn^{3+} ions in the ZBLAN– K_2MnF_6 (1 mol%) glass are shown in Table 1.

To verify the identification of Mn^{2+} bands, we used the Tanabe–Sugano diagram[19] for the d^5 (Mn^{2+}) electron configuration (Figure 4).

The Mn^{2+} band at 398 nm belongs to the transition to the $^4A_1$, $^4E(G)$ level, the energy of which is almost independent of the crystal field strength at small values of Δ/B. The value of E/B in the Tanabe–Sugano diagram is 32.4, which leads to a value of 776 cm^{-1} for the Racah parameter B at a transition energy of 25146 cm^{-1}. The band at 464 nm apparently belongs to a transition to the lowest excited level $^4T_1(G)$ (see Figure 4), for which the transition energy E is 21558 cm^{-1}; therefore, $E/B = 27.78$ for the $^4T_1(G)$ level at $\Delta/B = 0.726$. Using this value of Δ/B, we determined the positions of the other absorption bands (the calculation results are shown in parentheses in Table 1).

Thus, manganese in ZBLAN–K_2MnF_6 glass is present in the form of Mn^{2+} and Mn^{3+} ions, which indicates the reduction of Mn^{4+} ions introduced with K_2MnF_6 during glass synthesis. At comparable absorption band intensities of Mn^{2+} and Mn^{3+} (see Figure 3), the Mn^{2+} concentration is much higher than that of Mn^{3+} since the absorption of Mn^{3+} is associated with the spin-allowed transition $^5E \rightarrow {}^5T_2$, in contrast to the spin-forbidden transitions in Mn^{2+}. The reduction of Mn^{4+} can be caused by a high synthesis temperature (850–900 °C), at which equilibrium is strongly shifted towards

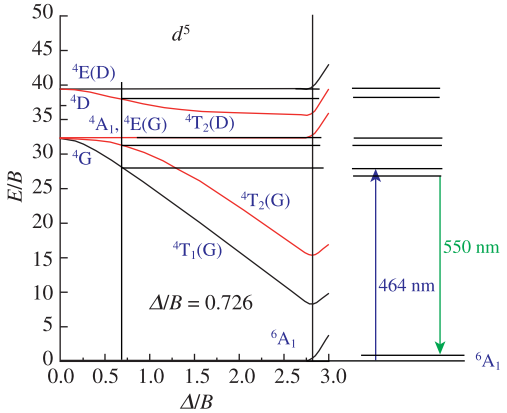

Figure 4 Part of the Tanabe–Sugano diagram for the d^5 (Mn^{2+}) electron configuration in ZBLAN.

the lower oxidation states of manganese. In addition, the relative concentrations of different manganese ions in glass can be affected by a ratio between their sizes and the sizes of ions that form the glass network. Mn^{2+} ions are considered to replace Ba^{2+} in the glass network structure.[20] The sizes of manganese ions (0.81, 0.72 and 0.68 Å for Mn^{2+}, Mn^{3+} and Mn^{4+}, respectively) are much smaller than that of Ba^{2+} (1.5 Å)[21], as is also indicated by the low crystal-field strength for the Mn^{2+} surrounding ($\Delta/B < 1$ in the Tanabe–Sugano diagram in Figure 4). The larger the valence of the ion, the greater the difference in the ion sizes; thus, divalent ions have an advantage over trivalent and tetravalent ions when incorporated into the glass network.

This research was funded by the Russian Science Foundation (RSF), grant no. 18-13-00407.

References

1 A. Piquette, W. Bergbauer, B. Galler and K. C. Mishra, *ECS J. Solid State Sci. Technol.*, 2016, **5**, R3146.
2 Z. Zhou, N. Zhou, M. Xia, M. Yokoyama and H. T. (Bert) Hintzen, *J. Mater. Chem. C*, 2016, **4**, 9143.
3 A. G. Paulusz, *J. Electrochem. Soc.*, 1973, **120**, 942.
4 Y. K. Xu and S. Adachi, *J. Appl. Phys.*, 2009, **105**, 013525.
5 R. Hoshino, T. Nakamura and S. Adachi, *ECS J. Solid State Sci. Technol.*, 2016, **5**, R37.
6 D. Chen, Y. Zhou and J. Zhong, *RSC Adv.*, 2016, **6**, 86285.
7 H. Zhu, C. C. Lin, W. Luo, S. Shu, Z. Liu, Y. Liu, J. Kong, E. Ma, Y. Cao, R.-S. Liu and X. Chen, *Nat. Commun.*, 2014, **5**, 4312.
8 L.-L. Wei, C. C. Lin, M.-H. Fang, M. G. Brik, S.-F. Hu, H. Jiao and R.-S. Liu, *J. Mater. Chem. C*, 2015, **3**, 1655.
9 J. H. Oh, H. Kang, Y. J. Eo, H. K. Park and Y. R. Do, *J. Mater. Chem. C*, 2015, **3**, 607.
10 Y. Jin, M.-H. Fang, M. Grinberg, S. Mahlik, T. Lesniewsi, M. G. Brik, G.-Y. Luo, J. G. Lin and R.-S. Liu, *ACS Appl. Mater. Interfaces*, 2016, **8**, 11194.
11 F. Tang, Z. Su, H. Ye, M. Wang, X. Lan, D. L. Philips, Y. Cao and S. Xu, *J. Mater. Chem. C*, 2016, **4**, 9561.
12 M. N. Brekhovskikh, L. N. Dmitruk, L. V. Moiseeva and V. A. Fedorov, *Inorg. Mater.*, 2009, **45**, 1477.
13 M. N. Brekhovskikh, L. V. Moiseeva, S. Kh. Batygov, I. A. Zhidkova and V. A. Fedorov, *Inorg. Mater.*, 2015, **51**, 1348.
14 R. Verstraete, H. F. Sijbom, K. Korthout, D. Poelman, C. Detavernier and P. F. Smet, *J. Mater. Chem. C*, 2017, **5**, 10761.
15 M. N. Brekhovskikh, A. I. Popov, V. A. Fedorov and Yu. M. Kiselev, *Mater. Res. Bull.*, 1988, **23**, 1417.
16 S. Kück, S. Hartung, S. Hurling, K. Petermann and G. Huber, *Phys. Rev. B*, 1998, **57**, 2203.
17 P. Bhavani, T. V. Nagalakshmi, A. W. Iqbal and K. A. Emmanuel, *J. Appl. Chem.*, 2013, **2**, 328.
18 B. Padlyak, O. Vlokh, B. Kukliński and K. Sagoo, *Ukr. J. Phys. Opt.*, 2006, **7**, 1.
19 Y. Tanabe and S. Sugano, *J. Phys. Soc. Jpn.*, 1954, **9**, 776.
20 L. N. Feuerhelm, S. M. Sibley and W. A. Sibley, *J. Solid State Chem.*, 1984, **54**, 164.
21 R. D. Shannon and C. T. Prewitt, *Acta Crystallogr.*, 1969, **B25**, 925.

Received: 30th June 2021; Com. 21/6599